Supporting Information

Prestele et al. 10.1073/pnas.1009174107

SI Methods

Generation of PEX10, PEX2, and PEX12 Plants with Dysfunctional Zinc RING Finger (PEX10-ΔZn, PEX2-ΔZn, PEX12-ΔZn) in the GFP-PTS1 WT Background. The homozygous PEX10-ΔZn1-line of our former analysis (1) was crossed with homozygous *Arabidopsis* Columbia WT plants expressing GFP-PTS1 (2) to obtain PEX10-ΔZn1 × GFP-PTS1 plants. Selfing of the heterozygous F1 generation resulted in 1/16 of the F2 plants homozygous for both the overexpressed PEX10-ΔZn construct and for GFP-PTS1. F2 plants homozygous for PEX10-ΔZn were selected by their dwarfish phenotype in normal atmosphere and normal development under high CO_2; they exhibited no further segregation on kanamycin. Transcription of the endogenous WT *PEX10* and the mutated *pex10*-ΔZn cDNA that are distinguishable by a MbiI-restriction site within the mutated zinc finger were confirmed by RT-PCR as described (1).

The *pex10*-ΔZn-T7-, *pex2*-ΔZn-T7-, and *pex12*-ΔZn-T7 cDNAs were constructed with an N-terminal T7 tag and a triple glycine (Gly)-serine (Ser) linker between the T7 tag and the start codon by PCR and were transformed into *Arabidopsis* Columbia GFP-PTS1 WT plants (2).

The *pex10-ΔZn-T7* cDNA was constructed using pex10-ΔZn in pBI121 (1) as template with primers PEX10-T7-se1 (5′-ATATGCTAGC**ATGGCTTCTATGACTGGAGGACAACAAATGGGA**(GGATCT)$_3$ATGAGGCTTAATGGGGATTCG-3′) and PEX10-T7-se2 (5′-ATATGCTAGC**ATGGCTTCTATG-3**′) together with PEX10-T7-as (5′-AGAGCTCCTAAAAATCAGAATGATACAAAC-3′) in equimolar ratio. The T7 tag is shown in bold. A triple Gly-Ser linker is inserted between T7 tag and start codon. NheI and SacI restriction sites are underlined. The construct was cloned under control of the 35S promoter into the *Agrobacterium tumefaciens* vector pBIAscIBar conferring Basta resistance (3) and was transformed into GFP-PTS1 WT plants (PEX10-ΔZn-T7-GFP-PTS1 plants). Three independent primary transformants were chosen for further analysis. Homozygous lines were obtained in T3 progenies. Transcription of the *pex10-ΔZn-T7* cDNA was confirmed by RT-PCR using PEX10-T7-se2 primer annealing on the T7 tag and PEX10-T7-as and by digestion of the fragment with MbiI. Plants homozygous for PEX10-ΔZn-T7 exhibited a dwarfish phenotype in normal atmosphere and no further segregation on Basta.

For *pex2-ΔZn-T7*-cDNA, the motif C_2GLG_2C2, which was unable to coordinate zinc ions in the C_3HC_4 zinc finger of *pex2* cDNA, was created by mutating C3, C4, and C5 to G and H to L in analogy to the *pex10*-ΔZn mutations (Fig. S1). A Bpu10I restriction site was introduced within the *pex2* C_2GLG_2C2 motif to distinguish WT and mutated cDNA versions; an N-terminal T7 tag and a triple Gly-Ser linker were added, thus obtaining *pex2*-ΔZn-T7 cDNA, and the construct was transformed into GFP-PTS1 WT plants (pex2-ΔZn-T7-GFP-PTS1 plants). The PEX2 cDNA (AY064063, RAFL09-26-B11; RIKEN) was subcloned into pGEM-7Zf+ (Promega) using PEX2-pBI-sense (5′-ATCCCCGGGATGACGCCGTCTACGCCTGCAGACG-3′) and PEX2-pBI-antisense (5′-TTGAGCTCTTCATTCAACAATGGTAGGTTCTCAAC-3′) via *Sma*I/*Sac*I (underlined). The corresponding ΔZn version was created by "splicing by overlap extension" PCR (4) as described previously (1) using PEX2-ΔZn2-se (5′-**G**GTCAGC**T**CAG*G*TAC**G**GTTACTAC**G**GCATAAGGACCCGCTGCGC-3′) and PEX2-ΔZn-as (5′-GC**C**GTAGTAAC**C**GTACCTG**A**GCTGAC**C**AGGCAGAGCTATAAACGG-3′). Point mutations are shown in bold. The *Bpu*10I restriction site is underlined. The N-terminal T7 tag and the triple Gly-Ser-linker between T7 tag and start codon were added by PCR using PEX2-T7-se1 (5′-ATAGCTAGC**ATGGCTTCTATGACTGGAGGACAACAAATGGGA**-(GGATCT)$_3$ATGACGCCGTCTACGCCTGC-3′) in combination with PEX2-T7-se2 (5′-ATAGCTAGC**ATGGCTTCTATG**-3′) and PEX2-as (5′-AGAGCTC TCATTTGCCACTTGAAACACC-3′) in equimolar ratio. (The T7 tag is shown in bold, and *Nhe*I and *Sac*I restriction sites are underlined.) The construct was cloned under control of the 35S promoter into the *Agrobacterium tumefaciens* vector pBIAscIBar conferring Basta resistance (3) and was transformed into GFP-PTS1 WT plants (PEX2-ΔZn-T7-GFP-PTS1 plants). Three independent primary transformants were chosen for further analysis. Homozygous lines were obtained in T3 progeny. The WT PEX2-cDNA with T7 tag and Gly-Ser linker was transformed in a similar manner into *Arabidopsis* Columbia GFP-PTS1 plants as a control. Transcription of the *pex2-ΔZn-T7* cDNA and the*PEX2*- WT-T7 cDNA, respectively, were confirmed by RT-PCR using PEX2-T7-se2 primer annealing on the T7 tag and PEX10-T7-as and by digestion of the fragment with *Bpu*10I that distinguishes *PEX2*-WT and *pex2*-ΔZn cDNA. Expression of GFP was confirmed by RT-PCR and confocal laser scanning microscopy (CLSM). T1 seeds of the Basta-resistant primary transformants segregated on Basta-containing Murashige and Skoog agar. Systematic CLSM analysis of rosette leaves of the 75% surviving seedlings homozygous or heterozygous for the *pex2*-ΔZn cDNA revealed that 25% exhibited a subcellular phenotype. The lines were identified as homozygous in the T2 generation.

For *pex12*-ΔZn-T7 cDNA, the motif C3G2 (unable to coordinate a zinc ion in the C5 zinc finger) was created by mutating C4 and C5 to G (Fig. S1). PEX12-WT-T7 cDNA was used as a control. A Kpn2I restriction site was introduced within the *pex12* C3G2 motif to distinguish WT and mutated cDNA transcripts; an N-terminal T7 tag was added, thus obtaining *pex12*-ΔZn-T7 cDNA, and the construct was transformed into GFP-PTS1 plants (pex12-ΔZn-T7-GFP-PTS1). The PEX12 cDNA clone BX824646 (INRA) missed the Adenin after Cytosin 746 bp downstream of the start codon, resulting in a frame shift. It was repaired by exchanging a 359-bp *Pfo*I/*Nco*I fragment from the cDNA clone AK117651 (RIKEN), which was truncated in the 5′ end. The resulting full-length cDNA was cloned into pGEM-7Zf+ (Promega) via *Bam*HI/ *Sma*I. The corresponding ΔZn version was created according to PEX2 using PEX12-ΔZn-se-*Kpn*2I (5′-GGATTTGTTTTC**G**GCTATTCCGGAGT ATTTAAGTATGTTTCAAAGTACAAGCG-3′) and PEX12-ΔZn12-as-*Kpn*2I (5′-ATACTTAAATACTCCGGAATAGC**C**GAAAACAAATCCAGAGACAGTGAC-3′) (the *Kpn*2I restriction site is underlined, and point mutations are shown in bold), together with PEX12-pBI-sense (5′-AAGGATCCATGTTGTTTCAGGTGGGAGGTG-3′) and PEX12-pBI-antisense (5′-CACCCGGGATAAATTTGATCAGTATATAAATTTT-3′) (*Bam*HI and *Sma*I sites are underlined). The N-terminal T7 tag was added by subcloning into pET28a(+) (Novagen) via *Bam*HI/*Xho*I. The pex12-T7 cDNA was amplified by PCR using PEX12-BglII (5′-TTTAGATCTAATGGCTAGCATGACTGGT-3′) and PEX12-Eco72I (5′-TTTCACGTGCCGGGATAAATTTGATCA-3′) (*Bgl*II and *Eco*72I restriction sites are underlined) and was cloned into the binary vector pCAMBIA1301 (Kan^R, Hyg^R; Cambia) and transformed into GFP-PTS1 WT (PEX12-ΔZn-T7-GFP-PTS1) plants. Three independent primary transformants were chosen for further analysis. Homozygous lines were obtained in T3 progenies. Transcription of the *pex12-ΔZn-T7* cDNA was confirmed by RT-PCR using PEX12-BglII and PEX12-Eco72I and by digestion of the fragment with *Kpn*I.

Transcription of GFP was confirmed by RT-PCR with primers EGFP-se-atg (5′-ATGGTGAGCAAGGGCGAG-3′) and EGFP-as-stop (5′-TCTTACTTGTACAGCTCGTC-3′) resulting in a 700-bp fragment and by CLSM of the leaves. Transcription of actin was used as control with primers actin-se (5′-ATGAAGATTAAGG-TCGTGGCA-3′) and actin-as (5′-TTCGAGTTTGAAGAGGC-TAC-3′) resulting in a 400-bp fragment.

All constructs were sequenced for control before transformation into *Agrobacterium tumefaciens*.

Quantitative RT-PCR. Total RNA was extracted from 7-d-old seedlings using the NucleoSpin RNA Plant kit (Macherey-Nagel) according to the manufacturer's instructions, and 2 μg of total RNA was subjected to cDNA synthesis using M-MuL V Reverse Transcriptase (Fermentas). DNAse treatment was performed during the extraction to avoid genomic DNA contamination. For quantification of the transcript level, two-step quantitative RT-PCR (qRT-PCR) was performed using the C1000 Thermal Cycler with a CFX96 Real-Time System (Bio-Rad Laboratories) and iQ SYBR Green Supermix (Bio-Rad Laboratories) with the cycling condition 95 °C for 10 min, 40 cycles of 95 °C for 10 s, 60 °C for 25 s The following primers were used for gene-specific amplification: PEX2 fw GGCAACTTGTGTGGAATGAA/PEX2 rv TCTTAACAGCTGAAGAGTTGAGCA; PEX10 fw TGGT-CTACCTCCGATTCAACTT/PEX10 rv GGTGCTGACGGGT-GCTTA; PEX12 fw CTCCAACAGTGTACCCTCCAC/PEX12 rv ATTCCTTCTTTGGCCATCTTT. For amplification of the T7 tag region, the following primers were used: T7-1 fw ATGGC-TTCTATGACTGGAGG/PEX2 rv-2 GCGAGAAGAGACTGC-GATT for PEX2ΔZnT7 in GFP-PTS1; T7-2 fw GGTGGAC-AGCAAATGGGT/PEX10 rv-3 CTGAGCTGCTAACGGGAAT for PEX10-T7 in pex10KO; T7-1 fw/PEX10 rv-2 ACCCG-AATCCCCATTAAG for PEX10ΔZnT7; and T7-2 fw/PEX12 rv-2 CGAAGGCTAGCAGGAAGT for PEX12ΔZnT7 in GFP-PTS1. For all samples, transcript levels were normalized against that of the ACT8 gene amplified using primers ACT8 fw TCAGCA-CTTTCCAGCAGATG/ACT8 rv CTGTGGACAATGCCTGG-AC. Parts of the primers were designed using primer design tools using the ProbeFinder software (https://www.roche-applied-science.com/sis/rtpcr/upl/index.jsp?id=UP030000) (Roche Applied Science).

Genomic Verification of PEX10-G93E, PEX10-P126S, and PEX10-W313* Targeting-Induced Local Lesions in Genomes lines. The point mutations in the targeting-induced local lesions in genomes (TILLING) lines were verified by PCR with primers PEX10-TILL-se (5′-TGAGTTTCCATGAGATTTTTGATTATTTG-3′) and PEX10-TILL-as (5′-AGTCTCAAAATAGGATTAACATATAACCTT-GT-3′) comprising the mutated sites. The mutation in PEX10-G93E [nucleotide G371A; Arabidopsis Biological Resource Center (ABRC) stock CS89852] gained the restriction site *Eam*1104I. The mutation in PEX10-W313* (nucleotide G938A; ABRC stock CS90121) lost the restriction site *Bse*NI. The mutation in PEX10-P126S (nucleotide C551T; ABRC stock CS92077) was controlled using the primer PEX10-TILL-as (see above) together with the primer PEX10-TILL-92077 (5′-TTTGTTCATATTGTACCAG-ACCGCGGTT-3′); the PEX10-TILL-92077 primer created a *Bsp*LI (GGNNCC) restriction site in the WT by conferring an A547G nucleotide exchange (underlined) that was not present in the PEX10-P126S line because of its C551T exchange, resulting in a 294-bp fragment that was cleaved to 267-bp and 27-bp fragments in WT and an uncleaved 294-bp fragment in the mutant line. PEX10-G93E remained heterozygous because of seedling lethality of homozygous plants (Fig. S3 *B* and *D*); homozygous plants could be obtained for PEX10-P126S (Fig. S3 *C* and *E*); loss of the zinc finger in PEX10-W313* led to embryo lethality of homozygous plants, as expected.

PEX10-G93E and PEX10-P126S Plants in the GFP-PTS1 WT Background. To clean the mutant background and to introduce GFP staining of peroxisomes, we crossed the PEX10-G93E and PEX10-P126S TILLING lines twice to WT ecotype Columbia lines expressing GFP-PTS1 (2); the point mutations were verified again by PCR.

Plant Growth Conditions. All seeds were surface sterilized in 80% ethanol, 0.1% Trition-X100 for 25 min; 3% NaOCl was added for 3 min followed by four washing steps with double-distilled H_2O, and seeds were plated on Murashige and Skoog medium (5). Seed dormancy was interrupted after 24 h at 4 °C. Germination was conducted at 22 °C in continuous light (250 μE m^{-2} s^{-1}). After 12 d, seedlings were transferred to soil (Fruhstorfer Einheitserde Type T) and grown either in the greenhouse or in phytochambers (Conviron) under long-day conditions (16 h light, 65% relative humidity, 22 °C/8 h darkness, 75% relative humidity, 18 °C). High CO_2 conditions of 1,800 ppm CO_2 partial pressure were adjusted in an open gas exchange system (6) including phytochambers (Conviron).

Enzyme Assays. All assays were measured in organelle pellets prepared as described (7). Serine-glyoxylate aminotransferase (8) and hydroxypyruvate reductase activity (9) were analyzed as described.

Photosynthetic Parameters. The photosynthetic yield was calculated from data collected with the portable pulse amplitude modulator fluorometer (PAM-2000; Walz) at 25 ± 1 °C and either ambient or 5-fold elevated CO_2 partial pressure (1); for details see Supporting Information in ref. 1.

Confocal Microscopy. Primary leaves of 3-wk-old homozygous T3 plants grown in Murashige and Skoog medium (5) were mounted under coverslips and analyzed using an Olympus FluoView FV1000 (Olympus), Argon laser excitation: 488 nm; emission: 500–530 nm (EGFP bandpass filter); 610–710 cy (3.5 bandpass filter, autofluorescence of chloroplasts); laser intensity 6%; PLABPO 40×/0.8 water objective.

Electron and Light Microscopy and Cytochemical Staining. Electron and light microscopy and cytochemical staining for catalase were performed as described previously (1, 10): Pieces of leaf tissue from 12-d-old plants were fixed with 2.5% glutaraldehyde in 75 mM sodium cacodylate, 2 mM $MgCl_2$, pH 7.0, for 1 h at 25 °C, rinsed several times in fixative buffer, and postfixed for 2 h with 1% osmium tetroxide in fixative buffer at 25 °C. After two washing steps in distilled water, the pieces were stained *en bloc* with 1% uranyl acetate in 20% acetone for 30 min. Dehydration and embedding in Spurr's low-viscosity resin was carried out. Ultra-thin sections of 50–70 nm were cut with a diamond knife and mounted on uncoated copper grids. The sections were poststained with aqueous lead citrate (100 mM, pH 13.0). Micrographs were taken with an EM 912 electron microscope (Zeiss) equipped with an integrated OMEGA energy filter operated in the zero loss mode. Specific localization of catalase activity was performed. For light microscopy semi-thin sections with a thickness of 500 nm were cut with a diamond knife, mounted onto glass slides, and embedded in epoxy resin. The focused ion beam (FIB) serial sectioning was performed by a Zeiss-Auriga workstation. The focused ion beam consists of Ga^+ ions accelerated by a voltage of 30 kV. The field emission scanning electron microscope (FESEM) column is mounted on top of the system chamber and the FIB column at an angle of 54°. In the cut-and-view mode, sections ranging in thickness from 15–25 nm (depending on the magnification) were produced with the FIB, and FESEM images were recorded at 2 kV using the in-lens energy-selective backscatter detector. Specimens were tilted at an angle of 54°; images were tilt-corrected for undistorted surface view.

Metabolome Analysis. Metabolome analysis was performed according to Wiekoop et al. (11). Frozen liquid nitrogen samples (10–15 mg) were homogenized in 2-mL Eppendorf tubes. One milliliter metabolite extraction buffer methanol/chloroform/water (2.5:1:0.5, vol/vol/vol) and 10 μL internal standard D-sorbitol-13C6 (200 μg/mL in H_2O) was added to the samples. By adding 0.5 mL double-distilled H_2O, vortexing, and centrifugation, the samples were separated into polar and lipophilic phases. The upper polar phase was dried completely in a SpeedVac concentrator (Savant), redissolved, and derivatisated for 90 min at 30 °C with 20 μL of 40 mg/mL methoxyamine hydrochloride in pyridine followed by 30 min at 37 °C with 90 μL N-Methyl-N-(trimethylsilyl)trifluoroacetamide. To determinate the retention time index (RI), 3 μL of an RI (n-alkanes C10–C36, each 200 μg/mL in pyridine) was spiked into the samples. GC coupled to a LECO Pegasus IV TOF (Leco Corp., Inc.) mass analyzer was used according to methods described in ref. 11. GC was performed on an HP 6890 gas chromatograph with deactivated standard split/splitless liners containing glass wool (Agilent). Sample 1-μL volumes were injected in splitless mode at 230 °C injector temperature. GC was operated on a VF-5ms capillary column, 30 m long, 0.25-mm inner diameter, 25-μm film thickness (Varian), at constant flow of 1 mL/min helium. The temperature program started with 1 min isocratic at 70 °C, followed by temperature ramping at 9 °C/min to a final temperature of 350 °C, which was held for 5 min. Scan rates of 20 s^{-1} and mass ranges of 70–600 Da were used. Raw data were deconvoluted with the ChromaTof software from LECO, which supports extraction of all mass spectra from a chromatogram, builds mass-spectral correction for coeluting metabolites, calculates the RIs, and identifies a suitable fragment mass for quantification. The processed data were analyzed by defining a reference chromatogram with the maximum number of detected peaks over a signal/noise threshold of 50. Afterwards, all chromatograms were matched against the reference with a minimum match factor of 800. Compounds were annotated by RI and mass spectra comparison with a user-defined spectra library (12). The peak area of the selected fragment ion from the individual metabolite on the mass spectrum of the gas chromatogram is quantified and normalized from the internal standard and by the fresh weight of the sample. This number is designated the "relative metabolite abundance." The relative abundance ratios can be compared directly by principal component analysis (PCA). The obtained comparison is valid only for samples from the same experiment. For the relative serine/glycerate ratios in Fig. S7, this limitation implies that the WT–mutant comparisons are exclusively valid within experiment *A*, *B*, *C*, or *D*; however, comparison of the WT relative serine/glycerate ratios between experiments (e.g., between experiments *A* and *C*) is not permissible.

Because several parallel experiments were made, SDs could be calculated. Not only are the relative ratios of Ser/glycerate in S7*A* for the PEX10-ΔZn1 mutant reduced; the ratio is disturbed also. This result allows the conclusion that the flux of the metabolites is disturbed, because Ser and glycerate are in different compartments.

Statistical Analysis. Univariate and multivariate data analysis was done with the TIGR MeV software version 4.1. As a first step, unsupervised classification via PCA was used to determine groups of samples and to recognize important factors in the data. Then, in a second step, differences between groups were analyzed via ANOVA and *t*-test clustering in supervised classification. The two-sided *t* test was performed with equal or unequal variance according to Welch's *t* test between two groups of samples. The ANOVA was performed according to the Fisher F-test, calculating significant differences in means of each metabolite separately across groups of samples.

1. Schumann U, et al. (2007) Requirement of the C3HC4 zinc RING finger of the *Arabidopsis PEX10* for photorespiration and leaf peroxisome contact with chloroplasts. *Proc Natl Acad Sci USA* 104:1069–1074.
2. Mano S, et al. (2002) Distribution and characterization of peroxisomes in Arabidopsis by visualization with GFP: Dynamic morphology and actin-dependent movement. *Plant Cell Physiol* 43:331–341.
3. Hoffmann T (2002) Signaltransduktion von Abscissinsäure in *Arabidopsis thaliana*: Transiente Expression in Protoplasten als Modellsystem. Dissertation (Institute of Botany. Technical University Munich, Munich, Germany).
4. Horton RM, Hunt HD, Ho SN, Pullen JK, Pease LR (1989) Engineering hybrid genes without the use of restriction enzymes: Gene splicing by overlap extension. *Gene* 77:61–68.
5. Murashige T, Skoog F (1962) A revised medium for rapid growth and bioassay with tobacco tissue culture. *Physiol Plant* 15:473–479.
6. Schnyder H, Schäufele R, Lötscher M, Gebbing T (2003) Disentangling CO_2 fluxes: Direct measurements of mesocosm-scale natural abundance $^{13}CO_2/^{12}CO_2$ gas exchange, ^{13}C discrimination, and labelling CO_2 exchange flux components in controlled environments. *Plant Cell Environ* 26:1863–1874.
7. Sautter C, Hock B (1982) Fluorescence immunohistochemical localization of malate dehydrogenase isoenzymes in watermelon cotyledons : A developmental study of glyoxysomes and mitochondria. *Plant Physiol* 70:1162–1168.
8. Häusler RE, Bailey KJ, Lea PJ, Leegood RC (1996) Control of photosynthesis in barley mutants with reduced activities in glutamine synthase and glutamate synthase. *Planta* 200:388–396.
9. Tolbert NE, Yamazaki RK, Oeser A (1970) Localization and properties of hydroxypyruvate and glyoxylate reductases in spinach leaf particles. *J Biol Chem* 245:5129–5136.
10. Wanner G, Vigil EL, Theimer RR (1982) Ontogeny of microbodies (glyoxysomes in cotyledons of dark-grown watermelon (*Citrullus vulgaris* Schrad.) seedlings. *Planta* 156:314–325.
11. Wiekoop S, Morgenthal K, Wolschin F, Scholz M, Selbig J, Weckwerth W (2008) Integration of metabolomic and proteomic phenotypes: Analysis of data covariance dissects starch and RFO metabolism from low and high temperature compensation response in *Arabidopsis thaliana*. *Mol Cell Proteomics* 7:1725–1736.
12. Kopka J, et al. (2005) GMD@CSB.DB: Fhe Golm Metabolome Database. *Bioinformatics* 21:1635–1638.

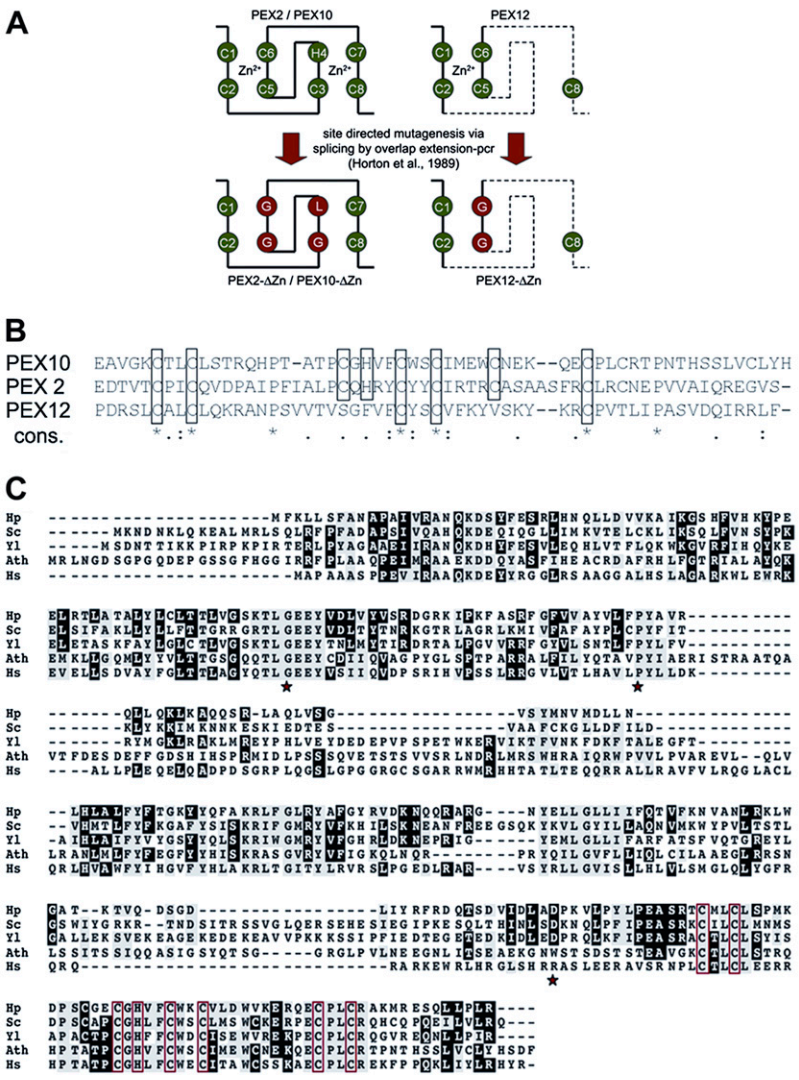

Fig. S1. The zinc RING finger motif in the C-terminal domain of PEX10, PEX2, and PEX12 and comparison of amino acid sequences of PEX10 peroxins. (*A*) WT and dysfunctional zinc finger. The amino acid changes resulting in a loss of zinc coordination sites are shown. (*B*) Alignment of the C_3HC_4 zinc RING finger in PEX10 and PEX2 and the C5 zinc RING finger in PEX12 of *Arabidopsis thaliana*. (*C*) Three SNPs within the coding region of *Arabidopsis* PEX10 are marked with stars: the first star indicates the mutation within the conserved TLGEEF motif; the second star indicates the mutation of the conserved proline; and the third star indicates the tryptophane mutated to a stop codon. The amino acids of the zinc-binding C_3HC_4 RING finger are framed in red. Conserved amino acids are shaded in black. Ath: *Arabidopsis thaliana*; Hp: *Hansenula polymorpha*; Hs: *Homo sapiens*; Sc: *Saccharomyces cerevisiae*; Yl: *Yarrovia lipolytica*.

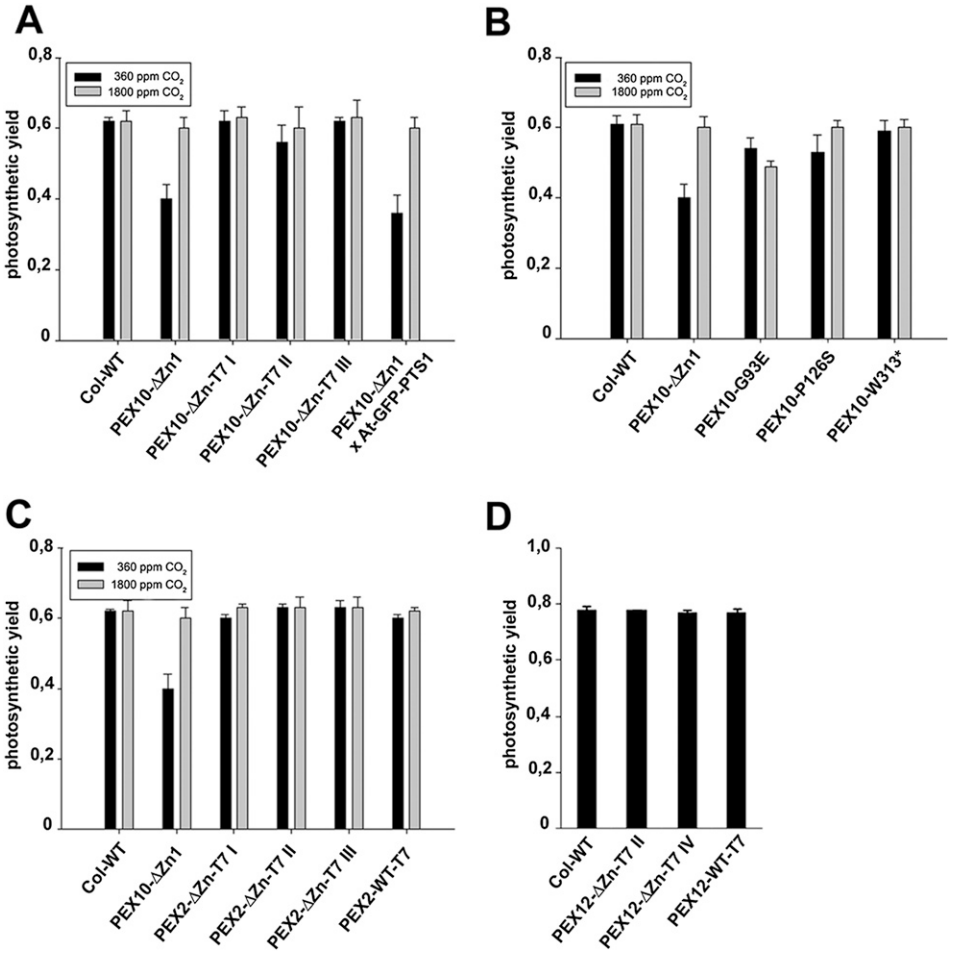

Fig. S2. Photosynthetic yield of photosystem II in light-adapted leaves after a saturating actinic light pulse. (*A*–*C*) PEX10-ΔZn1 and WT were used as control. Yield is decreased in PEX10-ΔZn1xAtGFP-PTS1 hybrids (*A*), whereas PEX10-ΔZn-T7 lines (*A*), heterozygous PEX10-G93E and PEX10-W313* and homozygous PEX10-P126S plants (*B*), and PEX2-ΔZn-T7 lines (*C*) exhibit no dramatic differences when grown under 360 ppm or 1,800 ppm CO_2. (*D*) PEX12-ΔZn-T7 and PEX12-WT-T7 transgenic lines exhibit no differences compared with WT plants when grown under 360 ppm CO_2.

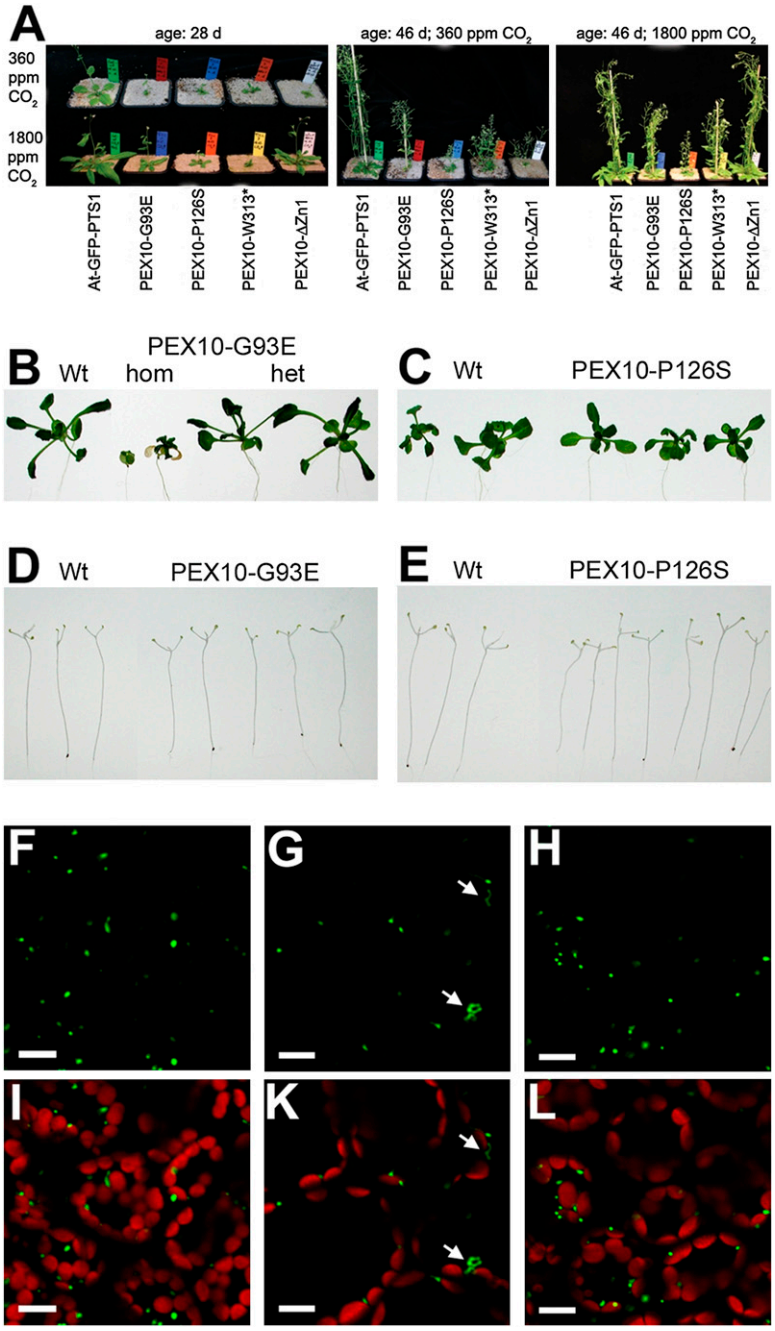

Fig. S3. Phenotype, peroxisome morphology and matrix protein import of PEX10-TILLING lines. (*A*) Phenotype of the PEX10-G93E, PEX10-P126S, and PEX10W313* TILLING lines grown under 360 ppm or 1,800 ppm CO_2. Plants are shown at an age of 28 d (*Left*: Upper row grown at 360 ppm; lower row grown at 1,800 ppm CO_2) and at 46 d (*Center*: Grown at 360 ppm CO_2), (*Right*: Grown at 1,800 ppm CO_2). Control plants: (*Left*) AtGFP-PTS1 WT; (*Right*) PEX10-ΔZn1. (*B* and *D*) The amino acid substitution G93E in PEX10 results in seedling lethality of homozygous plants when grown in the light. (*B*) Homozygous light-grown plants, shown at 14-d-old (*Center*), died a few days later and could not be rescued by high CO_2. (*D*) Dark-grown14-d-old PEX10-G93ExGFP-PTS1 hybrids display no difference in growth as compared with WT; 5 of 100 plants of a segregating line grown on agar plates are shown. (*C* and *E*) Homozygous PEX10-P126SxGFP-PTS1 plants exhibit slight growth retardation as compared with WT when grown in the light (*C*) but not in the dark (*E*). (*F–L*) Peroxisome morphology and matrix protein import in PEX10-G93E and PEX10-P126S mutants visualized by localization of GFP-PTS1. *Arabidopsis* 14-d-old secondary leaves are shown. (*F* and *I*) GFP-PTS1-WT. (*G* and *K*) PEX10-G93E mutant; arrows indicate deformed peroxisomes. (*H* and *L*) PEX10-P126S mutant. (*F–H*) GFP signal from peroxisomes. (*I–L*) GFP signal merged with chloroplast autofluorescence. (Scale bars, 10 μm.)

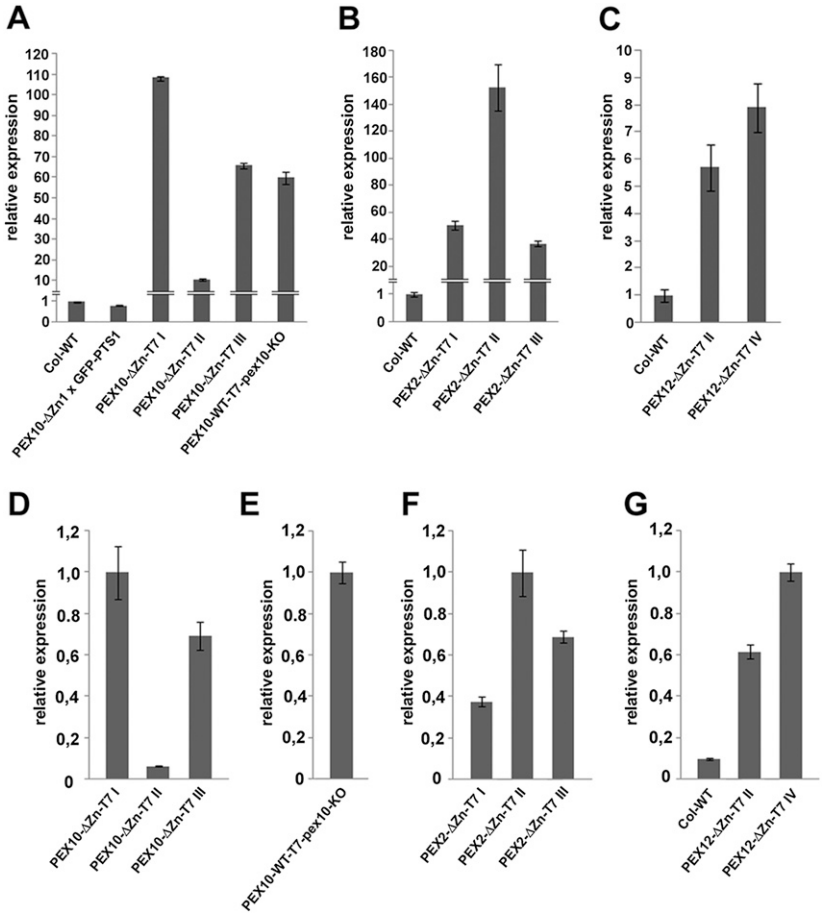

Fig. S4. Transcript levels of PEX10-, PEX2-, and PEX12 mutant lines. (*A*–*C*) Transcript levels of *PEX10* (*A*), *PEX2* (*B*), and *PEX12* (*C*) in the various transgenic lines were determined by qRT-PCR using gene-specific primers. *ACT8* was used as a reference gene for normalization of gene transcript levels in all samples. The data represent the mean normalized expression values of three technical replicates. The value of WT-GFP-PTS1 was set as 1. Error bars = SEM. (*D*–*G*) Transcript levels of *pex10*-ΔZn-T7 (*D*), *PEX10*-WT-T7 (*E*), *pex2*-ΔZn-T7 (*F*), and *pex12*-ΔZn-T7 (*G*) were determined by qRT-PCR using a T7 primer and a gene-specific primer. *ACT8* was used as a reference gene for normalization of gene transcript levels in all samples. The data represent the mean normalized expression of three technical replicates. Error bars = SEM.

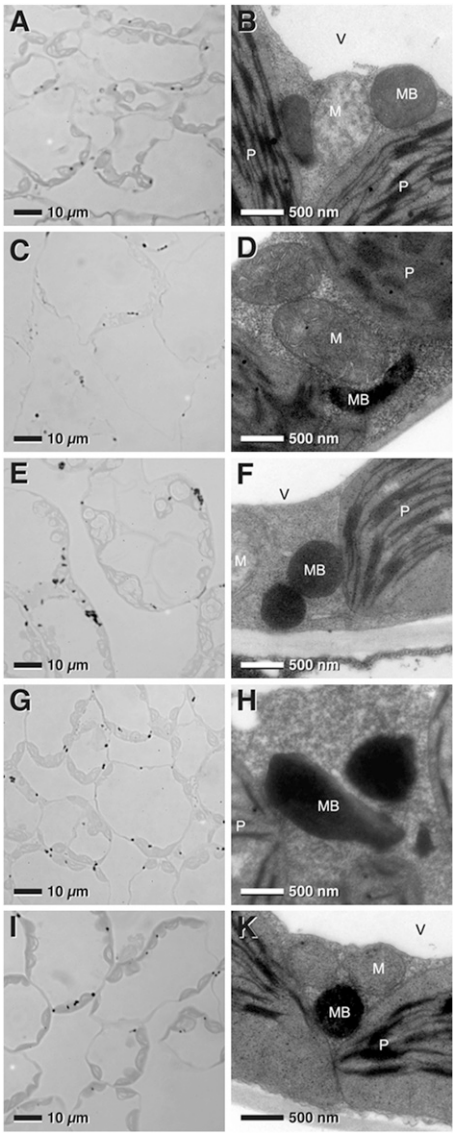

Fig. S5. Light and electron micrographs of 13-d-old leaf tissue of WT (*A* and *B*), PEX10-G93E (*C* and *D*), PEX10-P126S (*E* and *F*), PEX10-W313* (*G* and *H*), and PEX2-ΔZn-T7 (*I* and *K*) plants stained for catalase activity with diaminobenzidine. The leaf peroxisomes of WT, PEX10-P126S, and PEX2-ΔZn-T7 plants are ovoid and in physical contact with chloroplasts. PEX10-P126S peroxisomes sometimes are grouped and are slightly smaller than in WT plants; starch-filled plastids are conspicuous. PEX10-G93E and PEX10-W313* exhibit pleomorphic, elongated peroxisomes. M, mitochondrion; MB, microbody (peroxisome); P, chloroplasts; V, vacuole.

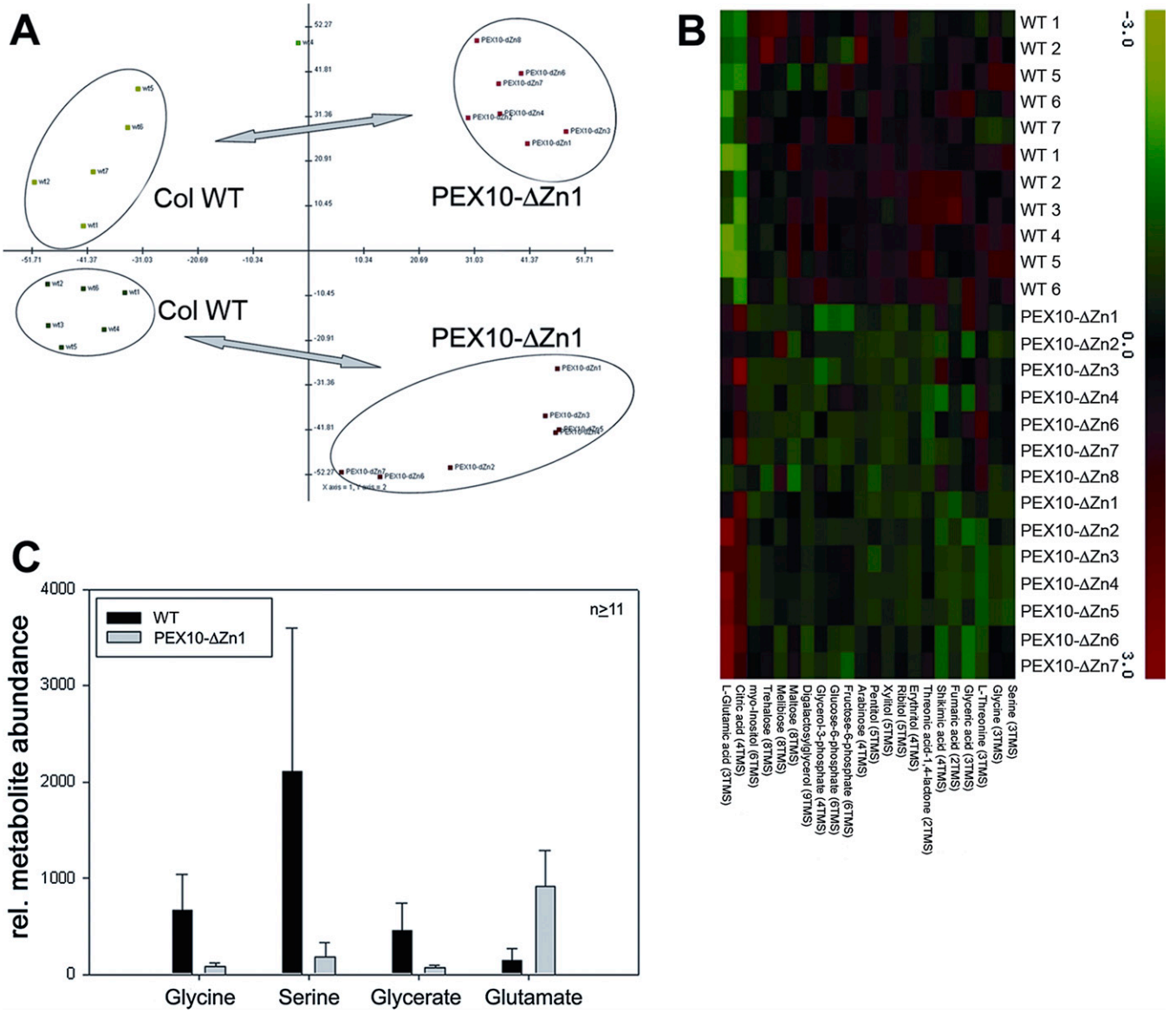

Fig. S6. Metabolome analysis of WT and PEX10-ΔZn plants confirms the impaired organelle contact. Plants were grown in normal air in the greenhouse (*A, Upper*) or in phytochambers (*A, Lower*). Four biological replicas with two technical replicas were analyzed for both experiments. (*A*) PCA with normalized metabolite data [x = (value-average)/SD] revealed a clear separation caused by different metabolite abundances. The first two principal components describe 46% of total variance. Each visualized point represents 77 quantitatively determined metabolites. (*B*) The *t*-test clustering reveals 22 metabolites with significant difference in abundance between WT and PEX10-ΔZn1 plants; red represents increased and green represents decreased metabolite levels. (*C*) Decreased levels of glycolate cycle metabolites Gly, Ser, and glycerate and elevated levels of Glu contribute highly significantly ($P < 0.001$, $n \geq 11$) to the difference between WT and PEX10-ΔZn1 plants.

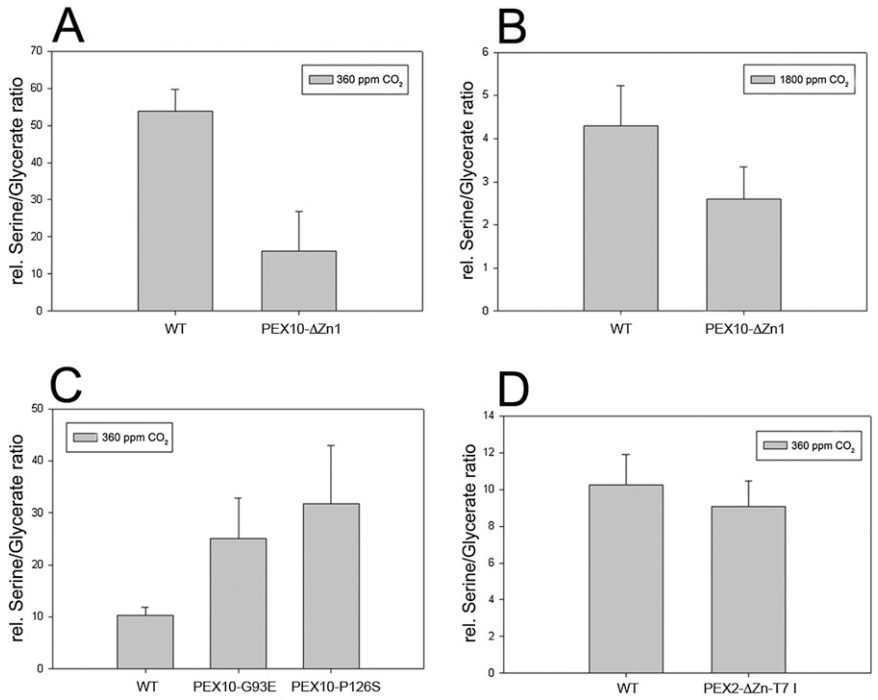

Fig. S7. Relative Ser/glycerate ratio as an indication for the metabolite flow within the glycolate cycle. (*A*) Significant reduction of the Ser/glycerate ratio in the PEX10-ΔZn1 mutant under normal atmospheric CO_2 conditions indicating a lack of Ser synthesis via the glycolate cycle ($P < 0.001$). (*B*) Significant reduction of the Ser/glycerate ratio in the PEX10-ΔZn1 mutant under high (1,800 ppm) CO_2 ($P < 0.01$). (*C*) Significant increase of the Ser/glycerate ratio in the PEX10 TILLING lines (G93E and P126S) ($P < 0.001$). (*D*) There is no change in the Ser/glycerate ratio in the PEX2-ΔZn-T7 mutant.

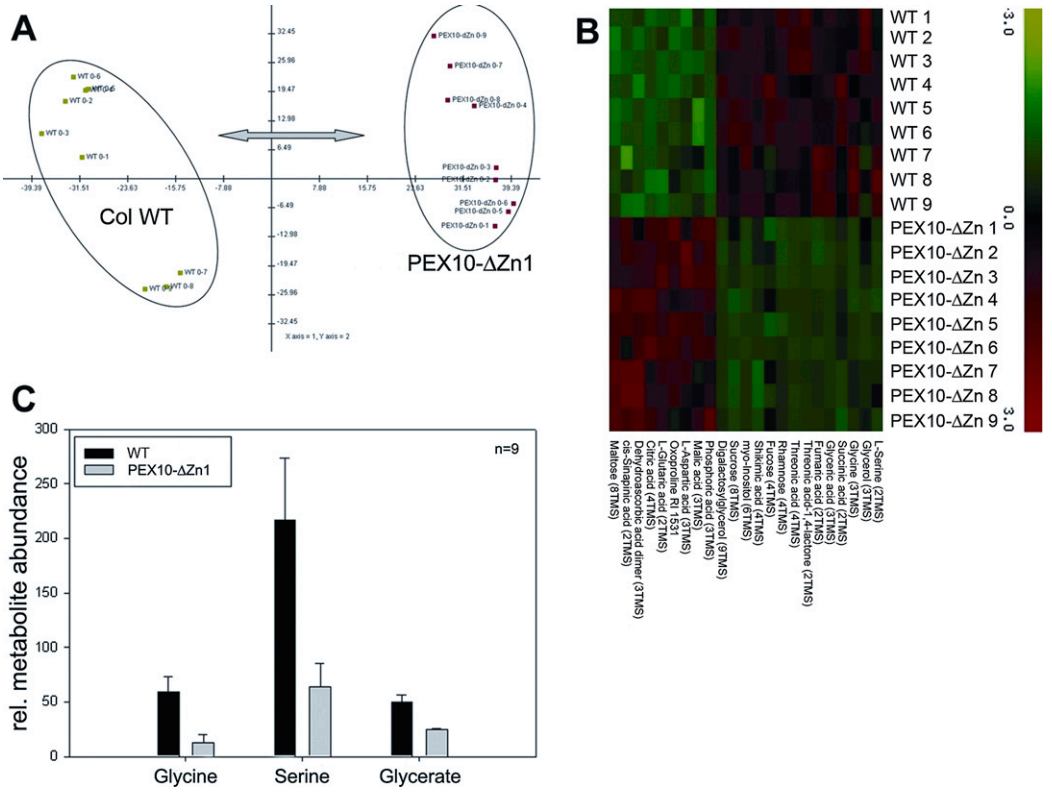

Fig. S8. Metabolome analysis of WT and PEX10-ΔZn1 plants grown under high CO_2 display a metabolic signature similar to that of plants grown under normal atmosphere. Three biological replicas with three technical replicas each were analyzed. (*A*) PCA with normalized metabolite data [x = (value – average)/SD] revealed a clear separation caused by different metabolite abundances. The first principal component describes 45.8% of total variance. Each point represents 55 quantitatively determined metabolites. (*B*) The *t*-test clustering illustrating significant changes of metabolite levels between WT and PEX10-ΔZn1 plants. The clustering visualizes the abundance of metabolites in each sample ranging from high (red) to average (black) to low (green). The metabolites of the glycolate cycle Gly, Ser, and glycerate contribute significantly to the separation of metabolite groups. (*C*) Decreased levels of the glycolate cycle metabolites Gly, Ser, and glycerate contribute significantly ($P < 0.001$) to the difference between WT and PEX10-ΔZn1 plants grown under nonoxidative stress conditions.

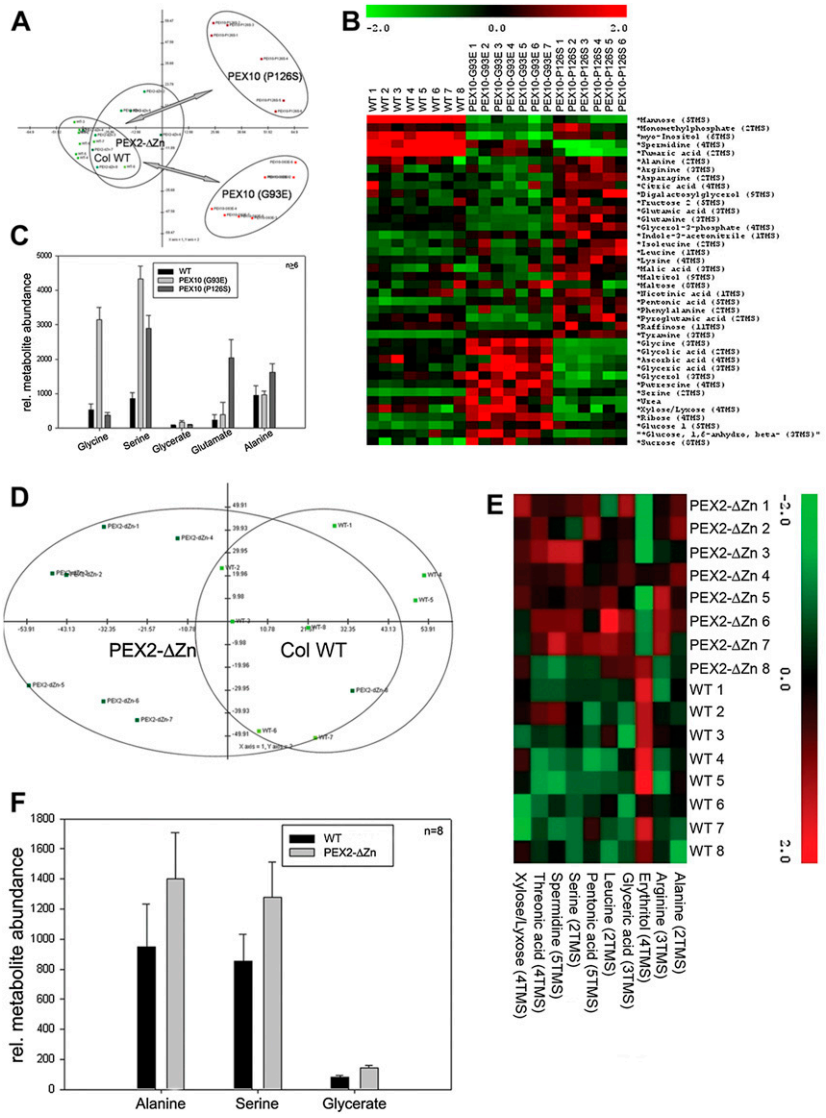

Fig. S9. Metabolome analysis of PEX10-G93E and PEX10-P126S mutants using PEX2-ΔZn-T7 plants as control (*A*–*C*) and PEX2-ΔZn-T7 plants (*D*–*F*). The amino acid substitutions in PEX10-G93E and PEX10-P126S mutants result in metabolite profiles different from WT. PEX2-ΔZn-T7 plants with their impaired import of matrix protein were included as controls. Plants were grown for 14 d in normal air. Six biological replicas were analyzed. (*A*) PCA with normalized metabolite data [x = (value-average)/SD] revealed a clear separation caused by different metabolite abundances for PEX10-G93E and PEX10-P126S, whereas WT and PEX2-ΔZn-T7 plants did not separate. The first principal component describes 27.5% and the second principal component 15.5% of total variance. Each visualized point represents 57 quantitatively determined metabolites. (*B*) ANOVA with integrated clustering reveals 40 metabolites with significant differences in abundance between the samples; red represents increased and green represents decreased metabolite levels. (*C*) In PEX10-G93E the glycolate cycle Gly, Ser, and glycerate levels are increased; in PEX10-P126S, only Ser is increased compared with WT ($P < 0.001$, $n \geq 6$). Metabolite levels of Gly, glycerate, Glu, and alanine (Ala) differ diametrically in the TILLING lines. Metabolome analysis in PEX2-ΔZn-T7 plants indicates no impairment of the glycolate cycle despite the reduced importation of peroxisome matrix protein. Average values from eight biological replicas are shown. (*D*) PCA with normalized metabolite data [x = (value-average)/SD] shows no separation because of the similar metabolite abundances. The first two principal components describe 41.1% of total variance. Each visualized point represents 57 quantitatively determined metabolites. (*E*) The *t*-test clustering reveals 10 metabolites with significant differences in abundance between WT and PEX2-ΔZn-T7 mutants; red represents increased and green represents decreased metabolite levels. The mutant exhibits enhanced values for Ser, Ala, and glycerate and thus is diametrically different from PEX10-ΔZn1 mutants. (*F*) The relative abundance of the glycolate cycle intermediates Ala, Ser, and glycerate is increased significantly in PEX2-ΔZn-T7 mutants ($P < 0.01$).

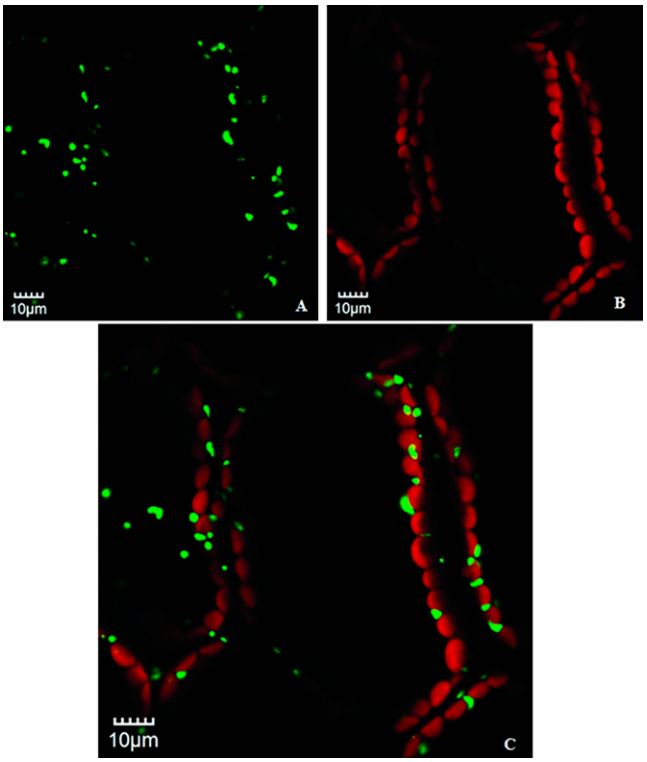

Movie S1. Still image from time-lapse movie "WT-GFP-PTS1_mesophyll cells" (Movie S1). Peroxisomes are stained with the peroxisome-localized GFP-PTS1. WT leaf peroxisomes are mostly spherical organelles appressed to the envelope of chloroplasts. (*A*) GFP signal of peroxisomes. (*B*) Autofluorescence of chloroplasts. (*C*) Merge.

Movie S1

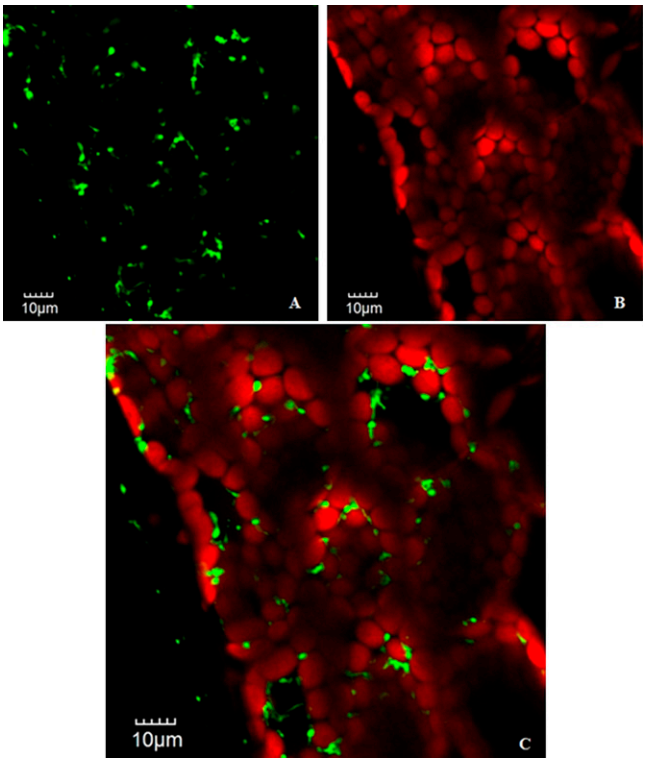

Movie S2. Still image from time-lapse movie "PEX10-ΔZnxGFP-PTS1_mesophyll cells" (Movie S2). Leaf-type peroxisomes in PEX10-ΔZn lines vary considerably in size and shape, are rarely associated with chloroplasts, and can move independently of chloroplasts. (*A*) GFP signal of peroxisomes. (*B*) Autofluorescence of chloroplasts. (*C*) Merge.

Movie S2